Springer

KSME

Journal of Mechanical Science and Technology 26 (2) (2012) 1099~1106
www.springerlink.com/content/1738-494x
DOI 10.1007/s12206-011-1215-0

Coupled linkage system optimization for minimum power consumption †

Kihan Shin[1], Sungcheul Lee[2], Hyunpyo Shin[1,*], Youngsun Yoo[3] and Jongwon Kim[1]

[1]*School of Mechanical and Aerospace Engineering, Seoul National University, Seoul, Korea*
[2]*Korea Institute of Machinery & Materials, Daejeon, Korea*
[3]*Doosan Technology Center, Doosan Infracore, Gyeonggi-do, Korea*

(Manuscript Received May 7, 2011; Revised August 15, 2011; Accepted October 8, 2011)

Abstract

This paper presents the dynamic analysis and kinematic parameter optimization of a coupled linkage system for the purpose of employing the system in construction industry. So far, the kinematic optimization of wheel loaders was approached heuristically rather than utilizing elaborate theoretical examinations due to the complexity of coupled linkage structures. The results of the theoretical analysis and kinematic parameter optimization are presented in this paper. A wheel loader with *Z*-bar linkage was analyzed. For a given end-effector path, the linkage system was optimized to carry out effective motion while exhibiting minimum power consumption during operation. A modified principle of reduced system was applied in order to execute the dynamics analysis of the coupled linkage system. As a result, an optimal *Z*-bar linkage structure and a distribution of power consumption within the given conditions were obtained.

Keywords: Coupled linkage; Dynamics analysis; Wheel loader; Optimization; Power consumption

1. Introduction

Various linkage structures exist for industrial purposes and environments. Linkage structures have been developed to satisfy different motion profiles of end-effectors [1]. An imperative objective to thoroughly consider during the linkage structure design stages is minimizing the required power consumption; power consumption is related to the capacity of actuator [2]. Linkage structures should also satisfy the required torque as well as the required movements for specific operations [3-5]. In addition, structures should be designed to maximize energy efficiency [6]. The culmination of the aforementioned requirements resulted in the development of industrial equipment that minimize torque and energy of the corresponding actuators [7-9].

Linkages connected directly or indirectly affect the platform of coupled linkage system structures. In general, most linkage systems are designed with a decoupled linkage structure due to advantageous characteristics, such as the relative ease when analyzing the torque distribution as well as attaining better control [10]. However, there exists a large amount of construction equipment that contains coupled linkage structures generating high torque at the end-effector within a compact space [11].

*Corresponding author. Tel.: +82 2 880 7144, Fax.: +82 2 875 4848
E-mail address: hpshin@rodel.snu.ac.kr
† Recommended by Associate Editor Jeong Sam Han

This paper examines the optimization of a coupled linkage system. A wheel loader, which is a typical piece of construction equipment utilizing a coupled linkage system, was chosen for the optimization. In particular, the *Z*-bar wheel loader is the most dominant model existing in construction industry. Because of its prevalence, the *Z*-bar linkage was employed during the linkage optimization. The purpose of conducting the optimization is to minimize the maximum power consumption of the prismatic actuators under certain constraints, such as the movement of a bucket. Minimizing the maximum power consumption provides the desirable outcome of reducing the actuator capacity of the wheel loader.

The optimization in this study comprises a kinematics analysis and a dynamics analysis in which a coupled linkage was disassembled into two serial chains using a modified principle of reduced system [12, 13]. For getting result easily, a branch stretching type exhaustive search method was applied to achieve fast convergence optimization. Finally, this paper presents an optimized linkage structure as well as a *Z*-bar wheel loader with minimum power consumption.

This paper is organized as follows. Section 2 describes the inverse kinematics and dynamics analyses of the wheel loader *Z*-bar linkage. The forward kinematics analysis and the Jacobian analysis for the *Z*-bar linkage are also introduced. Additionally, Section 2 presents the dynamics analysis of the non-redundant parallel mechanism incorporating the modified principle of reduced system. Section 3 briefly explains the branch stretching exhaustive search method. The optimization

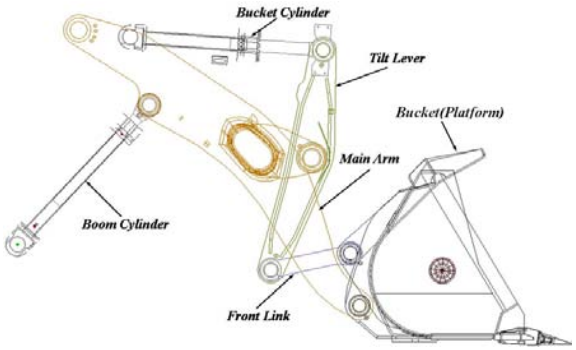

Fig. 1. Nomenclature of the *Z*-bar wheel loader.

constraints and the optimized results of the *Z*-bar wheel loader are shown in Section 4. Section 5 concludes the study.

2. Kinematics and dynamics analysis

This study investigated a method for optimizing a coupled linkage structure following a specific motion profile. For this purpose, a kinematics analysis and a dynamics analysis of the coupled linkage system using a Jacobian analysis in correlation with the modified principle of reduced system were necessary. A wheel loader containing the *Z*-bar linkage was the target of this optimization.

2.1 Linkage structure

For analyzing the kinematics of wheel loader, the linkage (front linkage) was regarded as a parallel mechanism, as shown in Fig. 1. The wheel loader contained two cylinders which controlled the height and rotation angle of the bucket, respectively. Throughout this paper, the platform means the bucket. The height of the bucket was determined by the boom cylinder, and the angle of bucket was determined by the bucket cylinder. However, the bucket angle changed due to the movement of the boom cylinder. The height was also affected by the bucket cylinder (Fig. 2). Because of these corresponding dependent movements, the linkage of the loader linkage was considered to be a coupled linkage structure.

The *Z*-bar linkage contains eleven joints: nine *R*-joints and two *P*-joints. Each joint was designated as A_1-A_{11}, as shown in Fig. 3. A_3 and A_8 are actuation joints with prismatic actuators. A_1, A_2, and A_7 are attached to the body of the loader. The location of bucket's center frame is indicated by {T}. L_{ij} represents the distance between *i*-joint and *j*-joint. And $q_{v1} - q_{v9}$ represent the rotation angles of each joint. The lengths of the cylinder were designated as q_{u1} and q_{u2}. θ_1-θ_3 are the fixed angles of the linkage.

The mass and inertia of each link were required in order to conduct the dynamics analysis. The front linkage system consisted of eight links, and cylinder was separated into two bodies, the base and the arm, for the analysis. In order to apply the modified principle of reduced system, the bucket was also separated into two links, the upper and the lower components, based on the center of mass.

(a) Moving motion of the front linkage

(b) DL400A of Doosan Infracore Co.

Fig. 2. Picture of wheel loader.

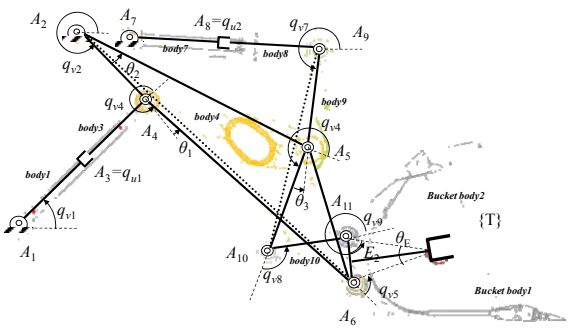

Fig. 3. Front linkage structure and assigned variables.

2.2 Kinematics analysis

The displacements of the actuators, which are independent joints, were designated as q_{u1}, q_{u2}, and the rotation angles of the dependent joints were named as $q_{v1} - q_{v9}$. The forward kinematics of the dependant joints is represented by the following Eqs. (1)-(9) when the independent joints q_{u1}, q_{u2} are given:

$$q_{v1} = \frac{\pi}{2} - \text{asin}\left(\frac{A_{2x} - A_{1x}}{L_{12}}\right) + \text{acos}\left(\frac{q_{u1}^2 + L_{12}^2 - L_{24}^2}{2q_{u1}L_{12}}\right) \quad (1)$$

$$q_{v2} = \pi + \text{acos}\left(\frac{\left(A_{2x} - A_{1x}\right)^2 + L_{12}^2 - \left(A_{2y} - A_{1y}\right)^2}{2\left(A_{2x} - A_{1x}\right)L_{12}} \right) + \text{acos}\left(\frac{-q_{u1}^2 + L_{12}^2 + L_{24}^2}{2L_{12}L_{24}} \right) \tag{2}$$

$$q_{v4} = 2\pi - \text{acos}\left(\frac{q_{u1}^2 - L_{12}^2 + L_{24}^2}{2q_{u1}L_{24}} \right) + \theta_1 \tag{3}$$

$$q_{v7} = \pi + \text{acos}\left(\frac{q_{u2}^2 + L_{59}^2 - L_{57}^2}{2q_{u2}L_{59}} \right) \tag{4}$$

$$q_{v6} = 2\pi + \text{acos}\left(\frac{L_{57}^2 + q_{u2}^2 - L_{59}^2}{2L_{57}q_{u2}} \right) + \text{asin}\left(\frac{A_{2y} + L_{25} \times \sin\left(q_{v2} + \theta_2\right) - A_{7y}}{L_{57}} \right) \tag{5}$$

$$q_{v4} = q_{v6} + q_{v7} - q_{v2} - \theta_2 - \theta_3 \tag{6}$$

$$q_{v8} = \left(\phi - \text{acos}\left(\frac{L_{510}^2 + L_{610}^2 - L_{56}^2}{2L_{510}L_{610}} \right) \right) + \text{acos}\left(\frac{L_{1011}^2 + L_{610}^2 - L_{611}^2}{2L_{1011}L_{610}} \right) \tag{7}$$

$$q_{v9} = \pi + \text{acos}\left(\frac{L_{1011}^2 + L_{611}^2 - L_{610}^2}{2L_{1011}L_{611}} \right) + \theta_{E2} \tag{8}$$

$$q_{v5} = \theta_2 - 4\pi + q_{v4} + q_{v8} + q_{v9} + \theta_E - \theta_1 \,. \tag{9}$$

The location of center of platform, A_E, is:

$$A_E = \begin{bmatrix} A_{2x} + L_{24}\cos\left(q_{v2}\right) + L_{46}\cos\left(q_{v2} + \theta_1\right) + L_{E6}\cos\left(q_{v2} + \theta_1 + q_{v5}\right) \\ A_{2y} + L_{24}\sin\left(q_{v2}\right) + L_{46}\sin\left(q_{v2} + \theta_1\right) + L_{E6}\sin\left(q_{v2} + \theta_1 + q_{v5}\right) \end{bmatrix}. \tag{10}$$

The Jacobian matrix is a time varying linear transformation matrix between dependent variable. Two Jacobian matrices are required for the *Z*-bar wheel loader: the constraint Jacobian matrix and the forward Jacobian matrix. The constraint Jacobian matrix is determined by differentiating the constraint equations. The constraint Jacobian matrix represents the velocity relationship between the independent and the dependent joints. The forward Jacobian matrix represents the relationship between the rates of the joint variable change and the platform velocity.

The dependent joint variable and the independent joint variable are given by:

$$q_{all} = \begin{bmatrix} q_1 & q_2 & q_3 & q_4 & q_5 & q_6 & q_7 & q_8 & q_9 & q_{10} & q_{11} \end{bmatrix}^T \tag{11}$$

$$q_{all} = U \begin{bmatrix} q_u \\ q_v \end{bmatrix} \tag{12}$$

$U \in \Re^{11\times11}$, $q_u \in \Re^{2\times1}$, $q_v \in \Re^{9\times1}$

where U is the relocation matrix, which is used to reassign the order of the independent and dependent joint vectors into an ascending order of the joint vector, q_{all} .

$$g(q_{all}) = \begin{bmatrix} g_1 & g_2 & g_3 & g_4 & g_5 & g_6 & g_7 & g_8 & g_9 \end{bmatrix}^T = 0 \tag{13}$$

where g(·) is the kinematic constraint equation. The velocity relationship between independent and dependant joints can be calculated using Eq. (13). Using the chain rule, the constraint equation transforms to constraint Jacobian, *Φ*.

$$\frac{dg}{dt} = \frac{dg}{dq_u}\frac{q_u}{dt} + \frac{dg}{dq_v}\frac{q_v}{dt} = \begin{bmatrix} G_u & G_v \end{bmatrix}\begin{bmatrix} \dot{q}_u \\ \dot{q}_v \end{bmatrix} = 0 \tag{14}$$

$$G_v\dot{q}_v = -G_u\dot{q}_u$$
$$\dot{q}_v = \Phi\dot{q}_u, \qquad \Phi \equiv -G_v^{-1}G_u \tag{15}$$

G_u is the constraint Jacobian matrix associated with the independent joint vector. Meanwhile, G_v is the constraint Jacobian matrix associated with the dependent joint vector. The linear velocity of the platform can be obtained by Eq. (16).

$$\dot{A}_E = \frac{dA_E}{dt} = (J_u + J_v\Phi)\dot{q}_u = J\dot{q}_u$$
$$J_u = \frac{dA_E}{dq_u}, \qquad J_v = \frac{dA_E}{dq_v}, \qquad J = J_u + J_v\Phi \tag{16}$$

where J is the forward Jacobian matrix. To acquire the acceleration relationship between the independent joints and the dependent joints, the constraint equation should be differentiated twice.

$$\dot{G}\dot{q} + G\ddot{q} = \dot{G}_u\dot{q}_u + \dot{G}_v\dot{q}_v + G_u\ddot{q}_u + G_v\ddot{q}_v = 0 \tag{17}$$

Then, we can obtain the relationship through several calculations as Eq. (18).

$$-G_v^{-1}\dot{G}\dot{q} + \Phi\ddot{q}_u - \ddot{q}_v = 0$$
$$\Psi = -G_v^{-1}\dot{G}, \quad \ddot{q}_v = \Psi\Lambda\dot{q}_u + \Phi\ddot{q}_u$$
$$\Omega = \begin{bmatrix} I_{2\times2} \\ \Psi \end{bmatrix}, \qquad \ddot{q} = \Lambda\ddot{q}_u + \Omega\Lambda\dot{q}_u \tag{18}$$

With these results, the joint velocity and the acceleration of the whole system can be calculated based on the independent joints.

2.3 Dynamics analysis

Actuating torque calculations are required for accurate power distribution calculations. The procedure comprising the dynamics analysis is an imperative analysis to conduct because of the wheel loader linkage's heavy weight. The dy-

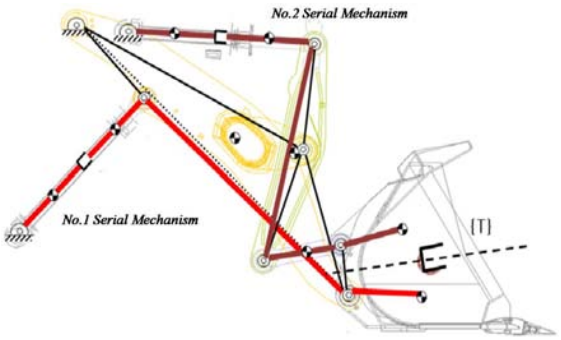

Fig. 4. Schematics of the reduced system of front linkage.

namic analysis should take into consideration the weights of the bucket and the sand; in combination, these weights occasionally exceed the weight of the linkage structure.

A possible approach considered for this experiment consists of the following aspects. The front linkage structure of wheel loader can be regarded as a parallel mechanism. The modified principle of reduced system is applied to analyze the dynamics of the parallel mechanism. In general, the reduced system can be obtained by cutting certain passive joints [14]. A disadvantage exists when utilizing this method. The joint torque occurring in the cut join does not appear in the motion equation [12]. Thus, when examining the front linkage of wheel loader, the modified reduced system in which the links are cut instead of joints was chosen as the means to analyze the dynamics of the system [13].

To obtain the general motion equation, the original system was separated into several open chain systems [15, 16]. The bucket was divided into two rigid bodies by the dotted line which was shown in Fig. 4. Each serial mechanism contains one cylinder, and had an upper or lower bucket platform. The dynamics equation of loader should be calculated through the reduced system. We assumed that all joints on the serial mechanisms possess a virtual actuator. The process to obtain the general motion equation was based on the studies performed by Cheng [16] and Ryu [17]. The dynamic equation of the reduced system is calculated by Eq. (19).

$$M^i(q^i)\ddot{q}^i + C^i(q^i,\dot{q}^i)\dot{q}^i + N^i(q^i,\dot{q}^i) = \tau^i,\ i = 1,2 \tag{19}$$

where q^1=[q_1 q_3 q_4 q_6], q^2=[q_7 q_8 q_9 q_{10} q_{11}], τ^1=[τ_1 τ_3 τ_4 τ_6] and τ^2=[τ_7 τ_8 τ_9 τ_{10} τ_{11}] represent joint displacements or rotation angles and torques. $M^i(q^i)\ddot{q}^i$ is the inertia matrix, $C^i(q^i,\dot{q}^i)\dot{q}^i$ is the Coriolis matrix, and $N^i(q^i,\dot{q}^i)$ is the gravity matrix. The inertia matrix is represented by Eq. (20).

$$M_{ij}^i(\theta) = \sum_{j=1}^{n} J_{ij}^T(\theta) M_{ij} J(\theta) \tag{20}$$

where M_{ij} is diag ([m_{ij} m_{ij} m_{ij} I_{ijx} I_{ijy} I_{ijz}]). m_{ij} is the mass of the i^{th} serial mechanism and the j^{th} link. I_{ijk} is the inertia of the i^{th} serial mechanism and the j^{th} link, k means axis of inertia. The body Jacobian, J_{ij}, is:

$$J_{ij} = \left|\xi_{i1}^{'} \ \cdots \ \xi_{ij}^{'} \ \ 0 \ \cdots \ 0\right|. \tag{21}$$

To obtain $\xi_{ij}^{'}$, we define ξ as:

$$\xi = \begin{bmatrix} v \\ w \end{bmatrix} \tag{22}$$

v indicates the translation axis when the joint is a prismatic joint. w indicates the rotation axis when the joint is rotation joint.

$\hat{\xi}$ is defined as $\begin{bmatrix} \hat{w} & \hat{v} \\ 0 & 0 \end{bmatrix}$, h is $\begin{bmatrix} R & p \\ 0 & 1 \end{bmatrix}$, and $Ad^{-1}h$ is $\begin{bmatrix} R^T & -R^T\hat{p} \\ 0 & R^T \end{bmatrix}$, we can get the vector $\xi_{ij}^{'}$ through the following equation:

$$\xi_{ij}^{'} = Ad^{-1}h_{ij}^n \cdot \xi_{ij},\quad n \le j \tag{23}$$

where h_{ij}^n is $e^{\xi_{i1}^{'}\theta_{i1}} \cdots e^{\xi_{ij}^{'}\theta_{ij}} h_{ij}(0)$.

Based on these calculations, the inertia matrixes of the two serial mechanisms were determined. The subsequent calculations regard the Coriolis matrix. Through differentiating the inertia matrix, the Christoffel symbol can be calculated through the following equation:

$$\Gamma_{ijk}^p = \frac{1}{2}\left(\frac{\partial M_{ij}^p}{\partial q_k} + \frac{\partial M_{ik}^p}{\partial q_j} - \frac{\partial M_{kj}^p}{\partial q_i}\right). \tag{24}$$

The Coriolis matrix is then achieved through the following:

$$C_{ij}^p = \sum_n \Gamma_{ijk}^p q_n \tag{25}$$

where i indicates the row, j indicates the column and p represents the number of the serial mechanism. The gravity matrix can be calculated from the partial-differentiation of the potential energy of each serial mechanism. The potential energy of each serial mechanism and the gravity matrix is shown Eq. (26).

$$\begin{aligned} V^i(q) &= \sum_j V_j^i(q) \\ N^i(q,\dot{q}) &= \frac{\partial V^i}{\partial q} \end{aligned} \tag{26}$$

The dynamics equation using the inertia can now be generated and the Coriolis and gravity matrix are Eq. (27). The velocity of bucket is very slow and actually, the contribution of the Coriolis term is nearly 1%, so the Coriolis term is ex-

cluded in the optimization process.

$$\begin{bmatrix} M_1 & \\ & M_2 \end{bmatrix}\begin{bmatrix} \ddot{q}_1 \\ \vdots \\ \ddot{q}_{11} \end{bmatrix}+\begin{bmatrix} C_1 & \\ & C_2 \end{bmatrix}\begin{bmatrix} \dot{q}_1 \\ \vdots \\ \dot{q}_{11} \end{bmatrix}+\begin{bmatrix} N_1 \\ N_2 \end{bmatrix}=\begin{bmatrix} \tau_1 \\ \vdots \\ \tau_{11} \end{bmatrix} \tag{27}$$

Substituting $q_{all}=U\begin{bmatrix} q_u \\ q_v \end{bmatrix}$ and multiplying U^{T}, Eq. (28) is obtained.

$$\begin{aligned} &U^T\begin{bmatrix} M_1 & \\ & M_2 \end{bmatrix}U\begin{bmatrix} \ddot{q}_u \\ \ddot{q}_v \end{bmatrix}+U^T\begin{bmatrix} C_1 & \\ & C_2 \end{bmatrix}U\begin{bmatrix} \dot{q}_u \\ \dot{q}_v \end{bmatrix} \\ &+U^T\begin{bmatrix} N_1 \\ N_2 \end{bmatrix}=\begin{bmatrix} \tau_u \\ \tau_v \end{bmatrix} \end{aligned} \tag{28}$$

In order to calculate the force exerted on the two cylinders, the dynamic equation of serial mechanisms must be converted to the entire linkage system using the relationship between the original system and the reduced system.

This relationship is shown as Eq. (29).

$$\begin{bmatrix} I \\ -\left(\dfrac{\partial g}{\partial q_v}\right)^{-1}\dfrac{\partial g}{\partial q_u} \end{bmatrix}^T \tau=\tau_u \tag{29}$$

The relationships of the velocity and the acceleration are substituted into the dynamics equation as Eq. (30)

$$\begin{aligned} &\Delta U^T\begin{bmatrix} M_1 & \\ & M_2 \end{bmatrix}U\Delta\ddot{q}_u+\Delta U^T\begin{bmatrix} M_1 & \\ & M_2 \end{bmatrix}U\Omega\dot{\Delta q}_u \\ &+\Delta U^T\begin{bmatrix} C_1 & \\ & C_2 \end{bmatrix}U\Delta\dot{q}_u+\Delta U^T\begin{bmatrix} N_1 \\ N_2 \end{bmatrix}=\tau_u\,. \end{aligned} \tag{30}$$

Then the final form of the dynamics equation can be shown simply as Eq. (31).

$$M(q_u)\ddot{q}_u+C(q_u,\dot{q}_u)\dot{q}_u+N(q_u,\dot{q}_u)=\tau_u \tag{31}$$

Consequently, the torque of the cylinders can be calculated once the values of the displacement, velocity, and acceleration of the cylinders are acquired.

3. Branch stretching type exhaustive search method

In general, kinematic parameter optimizations of parallel mechanisms are considered to be relatively difficult to apply analytic approaches because of their mathematical complexity. Besides the analytic approaches, two kinds of methods are used frequently. One is the exhaustive search method the other is the performance chart based method [18]. However, the performance chart based method mainly applied to the system with a limited number of kinematic parameter variable (less than five) because the parameter design space (PDS) cannot be expressed in a three-dimensional space, the exhaustive search method is chosen. The corresponding movements caused by the internal connections of the linkages of the coupled linkage system presents great difficulty when attempting to change the kinematic parameters of the linkages, as seen in Fig. 4. Additionally, the wheel loader's bucket should follow a specific path in this case. Thus, a conventional optimization method such as the Newton method cannot be easily applied to the optimization of the coupled linkage system. Therefore, we used an exhaustive search method for the optimization. However, this method requires a great amount of time in obtaining a precise optimal solution. In order to compensate for the difficulty posed by the excessive time, a method possessing a fast convergence characteristic is greatly desirable.

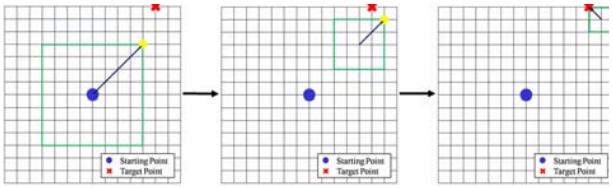

Fig. 5. Example of the branch stretching type exhaustive search method.

Thus, we applied a branch stretching exhaustive search method. Fig. 5 illustrates the optimization process progress comparing the values of the optimization index of the four points based on the starting point. Four points centered on the starting point were selected so that each point was located on a vertical orientation. After comparing the optimization index values one quasi-optimal point was selected and the selected point became the new starting point. Subsequently, the optimization process remained the same for the new starting point with the exception of the search radius. As the optimization procedure progressed, the search radius reduced to a smaller size than the preceding search radius.

The branch stretching type exhaustive search method can be used for the optimization of systems comprising many constraints as well as the optimization of complicated structures. This method possesses the accuracy of a conventional exhaustive search method with a relatively faster optimization speed. Thus, this method is appropriate for optimizing complex parallel mechanisms.

4. Optimization result

Using the results of the theoretical analysis and the aforementioned optimization method, we optimized the DL400A, *Z*-bar wheel loader of the Doosan Infracore which is shown in Fig. 2.

Table 1. Constraints and their values.

Constraint item	Value
Length of cylinder	Increased ***L***<0.8 max Cylinder ***L***
Height of gathering point (top)	4.35m
Max. back tilting angle (bottom)	42°
Max. back tilting angle (top)	59°
Max. fore tilting angle (top)	46°

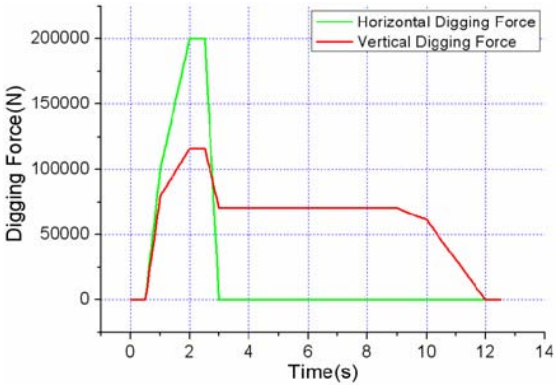

Fig. 6. Force exerted on the bucket.

4.1 Optimization index, constraint, and input value

Minimizing the maximum power consumption is related to the decrease in an engine's capacity, so it was selected as the optimization index. The wheel loader's power consumption can be written as the sum of the power of the boom cylinder and the power of the bucket cylinder. The optimization index is represented as:

$$\min I = \max(F_{boom\_cyl} \cdot v_{boom\_cyl} + F_{bucket\_cyl} \cdot v_{bucket\_cyl}). \quad (32)$$

The consumed power is composed of force F and velocity v. From the kinematic and dynamics analysis results of Section 2, utilizing virtual work theorem, F and v are obtained by Eq. (33).

$$\begin{aligned} &\tau_u^T dq_u = F^T dx \\ &\tau_u^T dq_u = F^T J dq_u \\ &F = J^{-T}\tau_u, v = J\dot{q}_u \end{aligned} \quad (33)$$

The bucket should follow a specific path. The path chosen is the real motion of the DL400 which is trained to the operator in digging and dumping process. Therefore, the path is not quite different with respect to the environment and operators.

Table 1 shows the constraints and bucket posture. In Table 1, the gathering point indicates the joint located at the lower part of the bucket. Input values are the initial joint locations, physical properties of the linkage, and the external force on bucket. In this study, we input the data of the force exerted on the bucket (force profile) as shown in Fig. 6. The introduced digging force profile is for the typical soil property case and it can vary according to the detail soil property. To optimize the kinematic parameters of the wheel loader's front linkage, we applied the typical digging force profile.

In Fig. 6, during 0~2 second, the digging force are increased rapidly because of wheel loader's forward moving and excessive amount of soil is put in which exceed the appropriate capacity of bucket. Then during 2~3 second, the bucket are elevated without forward moving of wheel loader and excessive amount of soil is poured out to the ground. As a result, the horizontal digging force is lowered to zero and also the vertical digging force is lowered a little. Finally, the wheel loader and its bucket are moved backward with the constant amount of soil until bucket's pour out motion. Based on these parameters and optimization conditions, the optimization of the loader's front linkage for minimizing maximum power consumption is performed.

Table 2. Joint coordinates of the original and the optimized models.

Joint coordinate	Target model (m)	Optimized model (m)
A1	(-0.466, 0.598)	(-0.405, 0.546)
A2	(0.000, 2.233)	(-0.145, 2.088)
A4	(0.537, 1.660)	(0.456, 1.666)
A5	(1.776, 1.258)	(1.800, 1.301)
A7	(0.393, 2.179)	(0.384, 2.238)
A9	(1.863, 2.079)	(1.791, 2.057)
A10	(1.464, 0.403)	(1.490, 0.414)
A6 (fixed)	(2.140, 0.130)	(2.140, 0.130)
A11 (fixed)	(2.071, 0.530)	(2.071, 0.530)

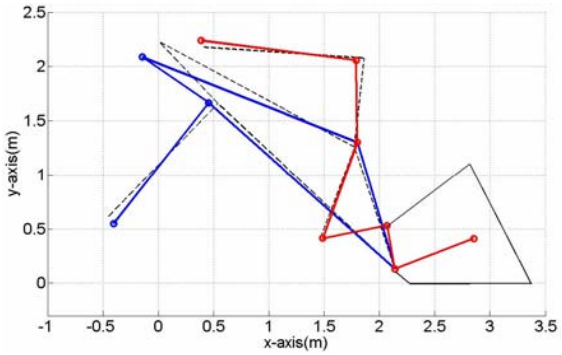

Fig. 7. Optimization result of the linkage structure.

4.2 Optimized wheel loader and its power distribution

Applying the constraints and the force profile, the optimization result was obtained and displayed in Fig. 7. Red and blue solid lines represent the shape of optimized loader. Black dotted line represents the original shape of the *Z*-bar wheel loader. To compare power consumptions between those linkages power distribution graph is plotted in Fig. 8.

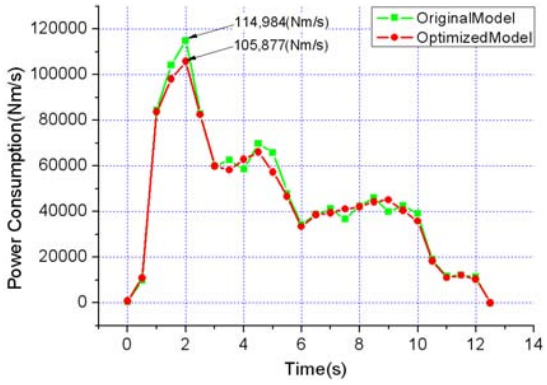

Fig. 8. Power distribution of the linkage structure.

The optimization results under the aforementioned constraint conditions illustrate a decrease of the maximum power consumption by 7.9%. Consequently, the engine capacity of the original *Z*-bar wheel loader can be downsized by that amount. In real industrial equipment, the production cost resulting from the amount of decrease of the maximum power consumption is valuable.

5. Conclusions

This paper presented the kinematics and dynamics analyses of a coupled linkage system, and the optimization of minimizing the maximum power consumption. For this purpose, the analysis of Jacobian matrix and dynamics of linkage using the modified principle of reduced system, and the optimization result of the linkage structure through branch stretching type exhaustive search methods were performed. Targeting DL400A, the power consumption of the original and the optimized model of *Z*-bar coupled linkage was obtained. Using this method, we can obtain the kinematic parameter optimization of a structure for minimizing the power consumption of the coupled linkage with a given moving path for the end-effector. The method used in this study can be applied to many other structures containing a coupled linkage system for minimizing the power and force.

Acknowledgment

This work was supported by a National Research Foundation (NRF) grant (No. 2009-0087640) and partly by the Korea Student Aid Foundation (KOSAF) grant (No. S2-2009-000-00308-1) funded by the MEST of the Korean government. The authors gratefully acknowledge this assistance.

References

[1] N. Sclater and N. P. Chironis, Mechanisms and Mechanical Devices Fourth Ed, *Mc Graw Hill Publishing Company*, New York, USA (2007).

[2] A. Bowling and O. Khatib, Dynamic loading criteria in actuator selection for desired dynamic performance, *Advanced Robotics*, 17 (7) (2003) 641-656.

[3] R. Saravanan and S. Ramabalan, Evolutionary bi-criteria optimum design of robots based on task specifications, *International Journal of Advanced Manufacturing Technology*, 41 (3/4) (2009) 386-406.

[4] J. A. Carretero and R. P. Podhorodeski, Kinematic analysis and optimization of a new three degree of freedom spatial parallel manipulator, *Journal of Mechanical Design*, 122 (17) (2000) 17-24.

[5] D. Park and S. Lee, Torque distribution using a weighted pseudoinverse in a redundantly actuated mechanism, *Advanced Robotics*, 17 (8) (2003) 807-820.

[6] K. S. Jeon and J. H. Park, Energy optimization of a biped robot for walking a staircase using genetic algorithms, *Proceeding of the ICCAS 2003* (2003) 215-219.

[7] R. Filla and A. Ericsson, Dynamic simulation of construction machinery, *Proceeding of the National Conference on Fluid Power*, 50 (2005) 429-438.

[8] M. Bohman, On Predicting Fuel Consumption and Productivity of Wheel Loaders, Master of science programme, Lulea University of Technology, Sweden (2006).

[9] H. Takahashi and Y. Morikawa, Study on the mechanism of over-head-type load-haul-dump with a vessel, *Journal of Terramechanics*, 41 (2/3) (2004) 175-185.

[10] V. Lippiello and L. Villani, An open architecture for sensory feedback control of a dual arm industrial robotic cell, *The Industrial Robot*, 34 (1) (2007) 46-53.

[11] S. Hirose and K. Arikawa, Coupled and decoupled actuation of robotic mechanisms, *Advanced Robotics*, 15 (2) (2001) 125-138.

[12] Y. K. Yiu and H. Cheng, On the dynamics of parallel manipulators, *Proceeding of the 2001 IEEE International Conference on Robotics and Automation* (2001) 3766-3771.

[13] W. A. Khan and V. N. Krovi, Recursive kinematics and inverse dynamics for a planar 3R parallel manipulator, *Journal of Dynamic Systems*, *Measurement, and Control*, 127 (4) (2005) 529-536.

[14] J. Wittenberg, Dynamics of Multibody Systems, B.G. Teubner, Stuttgart (1977).

[15] J. Kim, Motion planning for redundant parallel kinematic mechanism using joint torque distribution, Ph.D Dissertation, School of Mechanical and Aerospace Engineering, Seoul National University (2005).

[16] H. Cheng and Y. K. Yiu, Dynamics and control of redundantly actuated parallel manipulators, *IEEE/ASME Transactions on Mechatronics*, 8 (4) (2003) 483-491.

[17] S. J. Ryu, Joint torque distribution of redundantly actuated parallel mechanism, Ph.D Dissertation, School of Mechanical and Aerospace Engineering, Seoul National University (2001).

[18] Xin-Jun Liu, Jinsong Wang, A new methodology for optimal kinematic design of parallel mechanisms, *Mechanism and Machine Theory*, 42 (2007) 1210-1224.

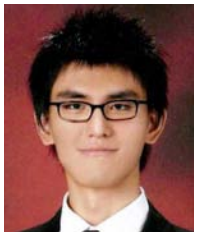

Kihan Shin received B.S. and M.S. degrees in School of Mechanical and Aerospace Engineering from Seoul National University, Seoul, Korea, in 2009, and 2011, respectively. Currently he is a senior associate at Samsung Construction and Trading. He researches automation robot for construction site and supports construction field related to rigging plan now.

Sungcheul Lee received B.S., M.S., and Ph.D degrees in School of Mechanical and Aerospace Engineering from Seoul National University, Seoul, Korea, in 2001, 2003, and 2008, respectively. Currently he is a senior researcher at Korea Institute of Machinery & Materials. His research interests include mechanism design, dynamics and design of experiment and their application to machining center and parallel mechanism.

Hyunpyo Shin received his B.S. degree in School of Biosystem Engineering, M.S., and Ph.D degrees in School of Mechanical and Aerospace Engineering from Seoul National University, Seoul, Korea, in 2002, 2004, 2009, respectively. Currently he is a senior researcher at Samsung Electro-Mechanics. His current research interests include design of redundantly actuated parallel mechanisms and medical robots.

Youngsun Yoo received his B.S. degree in Aerospace Engineering from Korea Aerospace University in 2002. Then, he received his M.S. degree in Automotive Engineering from Kookmin University, Korea, in 2006. He had worked in GM Korea as Vehicle Dynamic Engineer until 2010. Now he works in Doosan Infracore Co., Ltd as Dynamic Simulation Engineer of Construction Equipment.

Jongwon Kim received his B.S. degree in School of Mechanical Engineering from Seoul National University, Seoul, Korea, in 1978, his M.S. degree in mechanical and aerospace engineering from Korea Advanced Institute of Science and Technology (KAIST), Daejeon, Korea, in 1980, and his Ph.D degree in mechanical engineering from the University of Wisconsin, Madison, in 1987. He was with Daewoo Heavy Industry and Machinery, Korea, from 1980 to 1984. From 1987 to 1989, he was Director of Central Research and Development Division at Daewoo Heavy Industry and Machinery. From 1989 to 1993, he was a Researcher at the Automation and Systems Research Institute, Seoul National University. He is currently a Professor in the School of Mechanical and Aerospace Engineering, Seoul National University. His current research interests include parallel mechanism, Taguchi methodology, and field robots.